

Propagation of Tau Neutrinos and Tau Leptons through the Earth and their Detection in Underwater/Ice Neutrino Telescopes

Edgar Bugaev ^a, Teresa Montaruli ^{b,c}, Yuri Shlepin ^a,
Igor Sokalski ^{c,a,*}

^a*Institute for Nuclear Research, 60th October Anniversary Prospect 7a, 117312, Moscow, Russia*

^b*Physics Department, Bari University, Via Amendola 173, I-70126 Bari, Italy*

^c*Istituto Nazionale di Fisica Nucleare / Sezione di Bari, Via Amendola 173, I-70126 Bari, Italy*

Abstract

If muon neutrinos produced in cosmological sources oscillate, neutrino telescopes can have a chance to detect τ -neutrinos. In contrast to ν_μ 's the Earth is completely transparent for ν_τ 's thanks to the short life time of τ -leptons that are produced in $\nu_\tau N$ charged current interactions. τ -lepton decays in flight producing another ν_τ (regeneration chain). Thus, ν_τ 's cross the Earth without being absorbed, though losing energy both in regeneration processes and in neutral current interactions. Neutrinos of all flavors can be detected in deep underwater/ice detectors by means of Čerenkov light emitted by charged leptons produced in ν interactions. Muon and τ -leptons have different energy loss features, which provide opportunities to identify τ -events among the multitude of muons. Some signatures of τ -leptons that can be firmly established and are background free have been proposed in literature, such as 'double bang' events. In this paper we present results of Monte Carlo simulations of τ -neutrino propagation through the Earth accounting for neutrino interactions, τ energy losses and τ decays. Parameterizations for hard part and corrections to the soft part of the photonuclear cross-section (which contributes a major part to τ energy losses) are presented. Different methods of τ -lepton identification in large underwater/ice neutrino telescopes are discussed. Finally, we present a calculation of ν_τ double bang event rates in km^3 scale detectors.

Key words: energy losses, photonuclear interaction, tau neutrino, double bang, underwater neutrino telescope, oscillations

PACS: 14.60.Lm, 14.60.Fg, 96.40.Tv, 13.35.Dx

1 Introduction

$\nu_\mu \leftrightarrow \nu_\tau$ oscillations should lead to the proportion $\phi_{\nu_e} : \phi_{\nu_\mu} : \phi_{\nu_\tau} = 1 : 1 : 1$ for neutrinos produced in cosmological sources that reach the Earth, though the flavor ratio at production in typical sources is expected to be $\phi_{\nu_e} : \phi_{\nu_\mu} : \phi_{\nu_\tau} = 1 : 2 : 0$. Identification of UHE/EHE τ -events in deep underwater/ice Cerenkov neutrino telescopes (UNTs) [1–6] would confirm oscillations already discovered at lower energies [7–9]. Measuring the ratio between cosmological ν_μ and ν_τ fluxes one could also exclude or confirm some more exotic scenario [10,11], such as ν decay, in which $\phi_{\nu_\tau} \neq \phi_{\nu_\mu}$.

At energies $E_\nu \lesssim 1$ PeV a general approach to discriminate rare neutrino events from the huge amount of atmospheric muons present also at kilometer water/ice depths is to select events from the lower hemisphere. These can be produced by neutrinos, the only known particle that can pass through the Earth with negligible absorption below these energies. Nevertheless, ν cross-sections increase with energy. For muon neutrinos, absorption is considerable above 1 PeV, depending on the ν zenith angle, hence on the path-length transversed in the Earth. On the other hand, ν_τ 's generate τ -leptons via charged current (CC) interactions $\nu_\tau N \xrightarrow{CC} \tau N$ in the Earth. Being a short-lived particle, τ decays in flight producing another ν_τ and (in $\approx 35\%$ of the cases) secondary muon and electron neutrinos which are generated in decay modes $\tau \rightarrow e \nu_e \nu_\tau$ ($B_e=17.84\%$) and $\tau \rightarrow \mu \nu_\mu \nu_\tau$ ($B_\mu=17.36\%$) [12]. Thus, neutrinos of all flavors undergo a regeneration process and the Earth is transparent for ν_τ 's of any energy. Nevertheless, they loose energy through the Earth due to $\nu_\tau N$ interactions (CC and NC) where the hadronic showers take away part of the energy. A minor part of the energy is lost also due to τ -lepton propagation before decay. Thus, calculations for all flavor neutrino fluxes at detector location that result from propagation of an initial ν_τ flux through the Earth must necessarily take into account neutrino interaction properties, τ -lepton energy losses and τ -lepton decay. Such calculations are reported, e.g., in [13–20], both for monoenergetic ν_τ beams and for a variety of models for cosmological neutrino spectra.

τ -neutrinos can be detected in UNTs identifying τ leptons. To our knowledge the possibility of discriminating τ 's from muons through their different energy loss properties has not yet been analyzed. In this paper we discuss energy loss properties and specific τ -induced signatures, such as 'double bang' (DB) or 'lollipop' [21] events, which should be affected by negligible muon background. In [22] the results of a calculation of the number of DB events in an UNT are published, but authors considered only down-going ν_τ 's and ignored

* Corresponding author. Tel. +39-080-544-3225; fax: +39-080-544-2470.
Email address: Igor.Sokalski@ba.infn.it (Igor Sokalski).

those passing through the Earth to the detector from the lower hemisphere. In [14,23,24] the measurement of the ratio of up-going shower-like and track-like events is proposed, instead of an event-by-event identification of τ - or μ -events. As a matter of fact, τ -leptons, as well as muons, produce events of both kinds in a UNT. ν_e 's produce shower-like events, as well. In case ν_μ oscillate into ν_τ , the fraction of shower-like events is larger than what expected for no oscillations.

In this paper we describe the results, preliminarily given in [25,26], of a MC simulation of τ -neutrino propagation through the Earth. Both monoenergetic neutrino beams and spectra predicted by Protheroe [27] and Mannheim et al. [28] (which were not discussed in [14,15]) have been considered. We have taken into account corrections to photonuclear interaction cross-sections which play the main role in τ -lepton energy losses, compared to pair production and bremsstrahlung. We used results published in [29] where *i)* the soft part of photonuclear cross-section based on the generalized vector dominance model originally published in [30,31] is corrected and *ii)* the hard part is developed in the QCD perturbative framework. The soft part corrections to photonuclear interaction, not accounted for in [13–20], have lead to an increase of the total τ -lepton energy losses by 20–30% in UHE/EHE range. Also we have analyzed the possibility to distinguish UHE/EHE τ -leptons from muons in a UNT by different energy losses along tracks through production of electromagnetic and hadronic showers generated in bremsstrahlung, e^+e^- -pair production and photonuclear interaction.

In Sec. 2 we describe the tools used for this calculation with particular attention to τ -lepton energy losses for photonuclear interaction; in Sec. 3 results on propagation of UHE/EHE τ -neutrinos through the Earth are reported. In Sec. 4 we analyze the possibility to distinguish τ -lepton from muon in a UNT thanks to their different energy loss properties and we give results on a calculation of the rate of DB events coming from both hemispheres in km^3 scale UNTs; in Sec. 5 we conclude. In Appendix A the corrected formula for muon and τ -lepton photonuclear cross-section is given.

2 Tools for ν_τ propagation in the Earth

A MC calculation has been developed to account for the following processes:

- NC neutrino interactions that cause neutrino energy losses.
- CC interactions. For ν_e 's and ν_μ 's it has been assumed that resulting electrons and muons are absorbed, while for ν_τ 's τ -leptons are followed.
- τ -lepton propagation through the Earth accounting for its energy losses.
- τ -lepton decay resulting in another ν_τ appearance and in $\approx 35\%$ of the cases

also in ν_e or ν_μ production. ν_τ 's generated in τ decays have been reprocessed again through this chain of processes. Thus, the 'regeneration chain' $\nu_\tau \rightarrow \tau \rightarrow \nu_\tau \rightarrow \dots$ has been simulated.

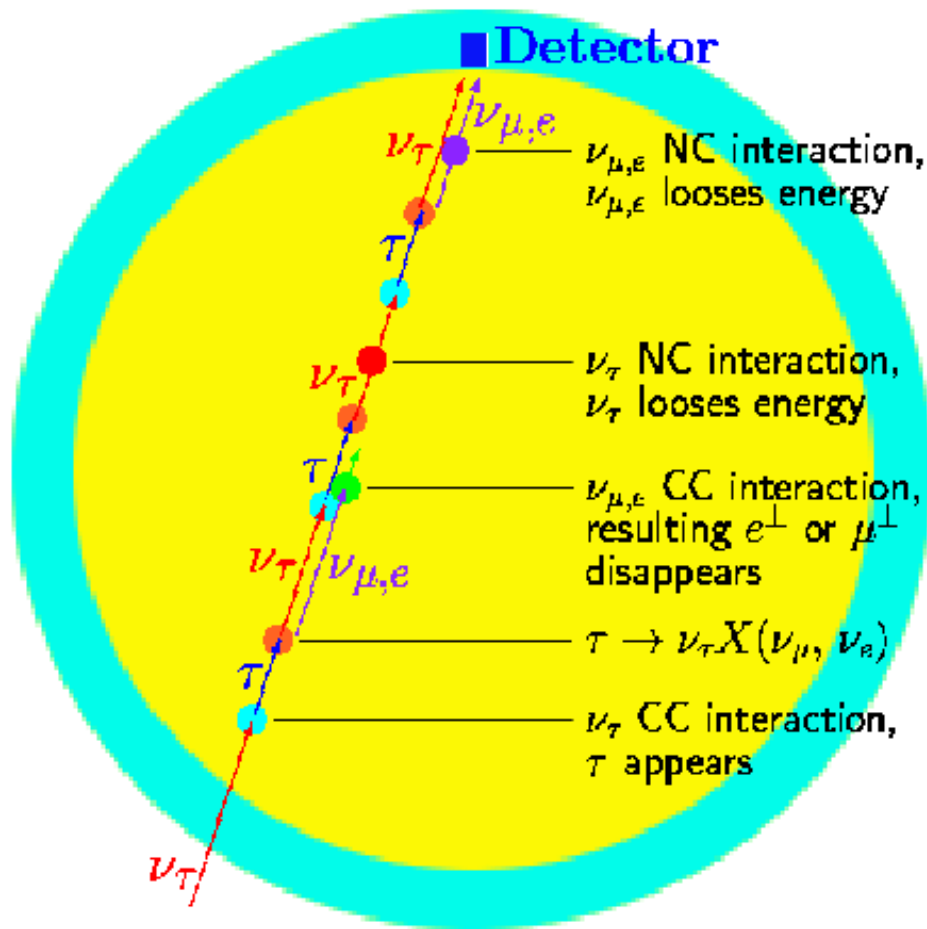


Fig. 1. Schematic view of processes induced by high energy ν_τ 's when propagating through the Earth.

We have assumed the Earth composition made by standard rock ($A=22$, $Z=11$) of variable density with the Earth density profile published in [32]. Processes undergone by τ -neutrinos during propagation through the Earth are shown schematically in Fig. 1.

2.1 Neutrino interactions

To simulate νN interactions we have used a generator developed by P. Lipari and F. Sartogo which is based on cross-sections described in [33]. It has been adapted for our use up to the high energy region we are interested in ($E_\nu > 10^5$ GeV) adjusting the efficiency of the rejection technique method described in [34]. Both for NC and CC interactions we have accounted only

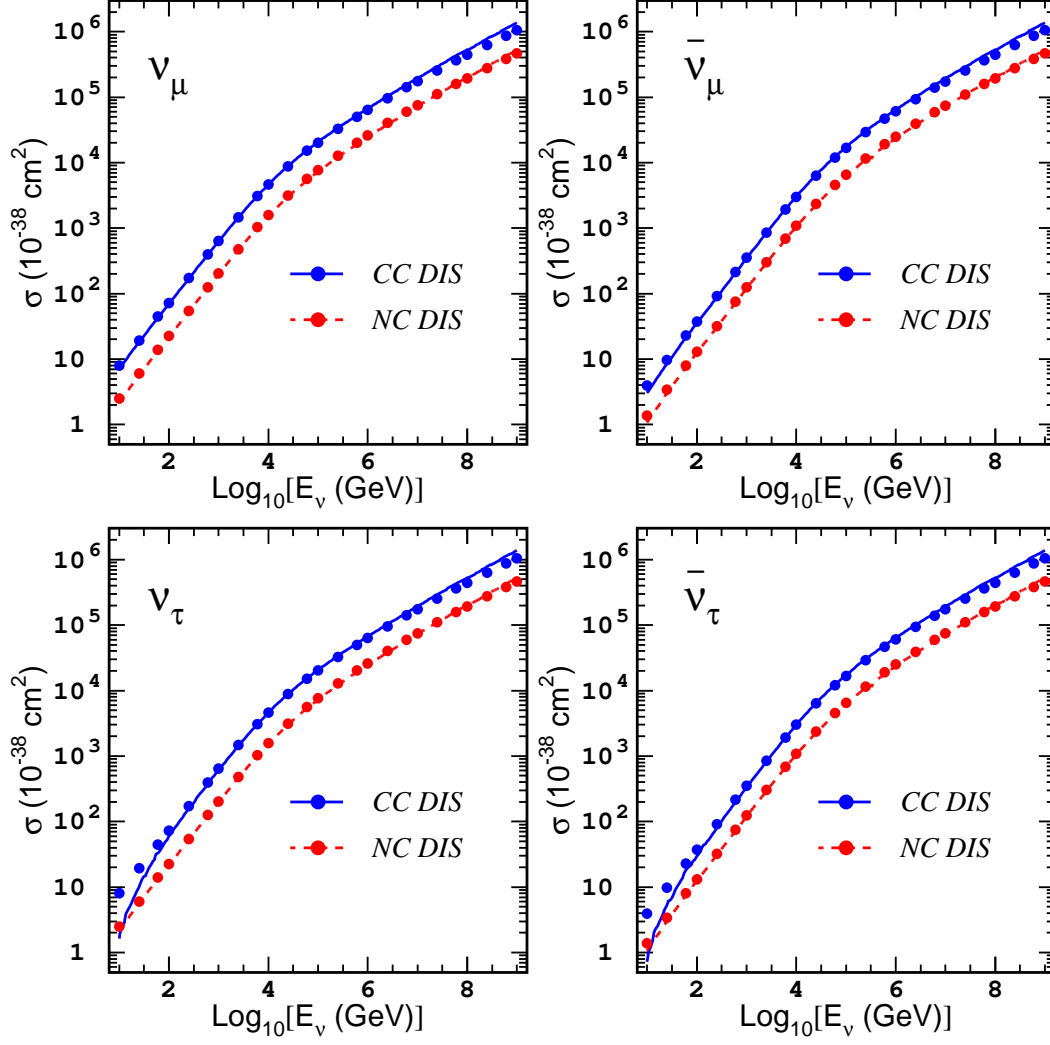


Fig. 2. CC (solid lines) and NC (dashed lines) deep inelastic scattering cross-sections for ν_τ , $\bar{\nu}_\tau$, ν_μ , and $\bar{\nu}_\mu$ (cross-sections for electron (anti-)neutrinos practically coincide with ones for muon (anti-)neutrinos for isoscalar medium with $Z/A = 0.5$). Lines: cross-sections with structure functions CTEQ3-DIS (used in this work); markers: cross-sections with CTEQ4-DIS (from [42]).

for deep inelastic scattering since in the considered energy range other channels contribute negligibly. For what concerns deep inelastic scattering, the generator uses the electroweak standard formula for the inclusive differential cross-section and it is based on the LUND packages for hadronization [34–36]. Structure functions CTEQ3-DIS [37] taken from PDFLIB [38] suited for the high energy regime have been used¹. More recent versions of CTEQ PDFs [39–41] produce differences on cross-sections at the level of up to 25% at 10^9 GeV (see Fig. 2).

¹ It should be noticed, however, that the CTEQ3 parton function extrapolation at small Bjorken x_{Bj} , as implemented in PDFLIB, is more similar to the CTEQ6 one rather than to the CTEQ4 and CTEQ5.

2.2 *Tau-lepton energy losses*

The MUM package (version 1.5) has been used to simulate τ -lepton propagation through matter. Comparing to [43] (where the first version of the package originally developed for the muon propagation was described) the package has been extended to treat τ -leptons, accounting for their short life time and large probability to decay in flight. Besides, the newest corrections to photonuclear cross-section have been introduced. Formulas for cross-sections for e^+e^- -pair production, bremsstrahlung, knock-on electron production and stopping formula for ionization implemented in MUM 1.5 can be found in [43] (Appendix A) ² where they are given according to [50–60].

Main improvements in MUM 1.5 concern photonuclear interaction of leptons with nucleons, in which virtual photons are exchanged. We are interested in the diffractive region of the kinematic variable space ($q^2 < 0$, transferred energy ν large, $x_{Bj} \sim q^2/2\nu$ small). The photonuclear interaction has been treated as the absorption of the virtual photon by the nucleon and, using the optical theorem, it has been connected with the Compton scattering of a virtual photon, $\gamma^* + N \rightarrow \gamma^* + N$. The Compton scattering in the diffractive region has been described by the vacuum exchange which, in turn, is modeled in QCD by the exchange of two or more gluons in a color singlet state. This is possible because, in the laboratory system, the interaction region has a large longitudinal size, and the photon develops an internal structure due to its coupling with quark fields. In the diffractive region, γ^*N -scattering dominates the Compton amplitude, while the contribution to it due to the photon bare component is smaller.

It has been shown by HERA experiments [61–66] that the picture of the usual soft diffraction, soft pomeron exchange, does not work well if the center-of-mass energy of γ^* and the target nucleon N is very large (i.e. if q^2 and ν are in the diffractive region). For a description of the data in the framework of the simplest Regge-pole model, one needs at least two pomerons: soft and hard ones. A two-component picture of the photonuclear interaction in the diffractive region arises very naturally due to inherent QCD properties (asymptotic freedom, confinement, color transparency) and is the common feature of some recent quantitative models [29,44,45]. Generally, the photonuclear cross-section integrated over $Q^2 = -q^2$ is expressed through the electromagnetic

² When dealing with τ -lepton propagation one must change muon mass for τ -lepton mass in all the formulas except for expression for $q_c = 1.9 m_\mu / Z^{1/3}$ in formula for bremsstrahlung cross-section (see page 074015-15, Appendix A in [43]) where the muon mass was introduced just as a mass-dimension scale factor.

structure functions of nuclei $\sigma_{L,T}$ by the formula

$$\frac{d\sigma^{pn}}{dv} = \frac{\alpha}{2\pi v} \int_{Q_{min}^2}^{\infty} \frac{dQ^2}{Q^2} \{v^2 \sigma_T (1 - \frac{2m_l^2}{Q^2}) + 2(1-v)(\sigma_T + \sigma_L)\}, \quad (1)$$

where $Q_{min}^2 \cong m_l^2 v^2 / (1-v)$, $v = \Delta E / E$ is the fraction of energy lost in the interaction by a lepton of energy E with mass m_l and $\alpha = 1/137$ is the fine structure constant.

In the first version of the MUM code [43] only the soft part of this integral was accounted for according to Bezrukov-Bugaev (BB) parameterization that was developed in the frame of the generalized vector dominance model [30,31]. In MUM 1.5 two main improvements have been done. Firstly, new terms have been included in the BB parameterization [29]. Since these produce negligible effects in the case of muon, they were not introduced in the original formula given in [30,31]. Nevertheless, these terms are essential in case of τ -lepton (due to its larger mass compared to muon: $m_\mu = 0.1057$ GeV; $m_\tau = 1.777$ GeV) and they increase total τ -lepton energy losses by $\sim 20 \div 30\%$ in UHE/EHE range. Secondly, the hard component of the photonuclear cross-section has been introduced using results obtained in [29]. This part is described by the phenomenological formula based on the color dipole model [46,47]. The main element of the approach used in [29] is the total cross-section $\sigma(r_\perp, s)$ for scattering of dipoles ($q\bar{q}$ -pairs) of a given transverse size r_\perp from a target proton at fixed center-of-mass energy squared s . The r_\perp -dependence of $\sigma(r_\perp, s)$ is qualitatively predicted by perturbative QCD:

$$\sigma(r_\perp, s) \sim r_\perp^2 e^{-\frac{r_\perp}{r_\perp^0}} (r_\perp^2 s)^{\lambda_H}. \quad (2)$$

In this formula λ_H and r_\perp^0 are parameters determined from a comparison of the total photonuclear cross-section (or structure functions) with HERA data at small x_{Bj} . Such an expression for $\sigma(r_\perp, s)$ was suggested in [48]. Besides, for a region of large s (outside of the HERA region) the unitarization procedure is used in [29], which leads, asymptotically, to a logarithmic s -dependence of the dipole cross-section,

$$\sigma^{unit}(r_\perp, s) \sim \lambda_H \ln s. \quad (3)$$

The hard part of the photonuclear cross-section is shown in Fig.4 and Fig.5 in [29] for muons and τ 's, respectively. We have made a polynomial parameterization for this part that is given in Appendix A along with the complete formula for photonuclear cross-section used in this work.

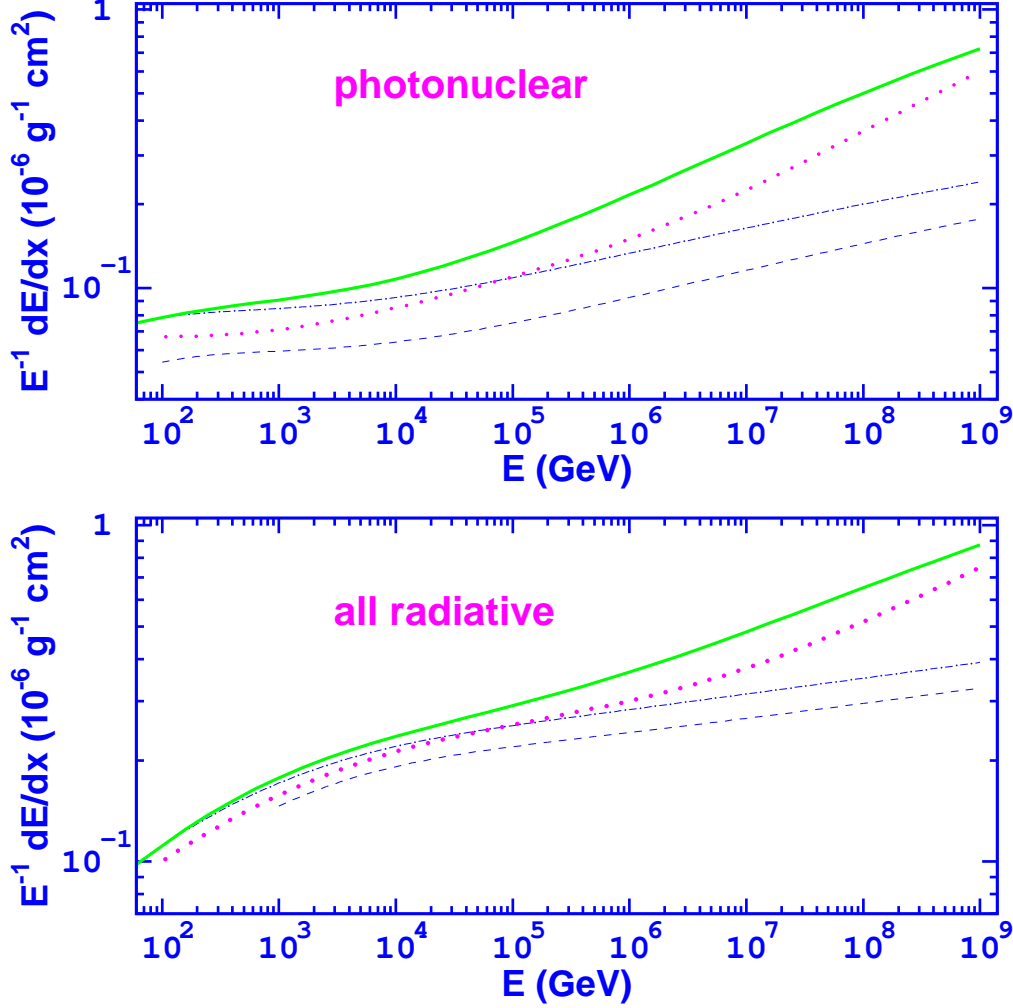


Fig. 3. τ -lepton energy losses in standard rock. Upper plot: energy losses due to photonuclear interaction. Lower plot: energy losses due to all radiative processes, including bremsstrahlung and direct e^+e^- -pair production computed according to [50–56]. In each plot: dashed line is for non corrected soft part [30,31]; dash-dotted line for corrected soft part [29–31]; dotted line includes hard component of photonuclear cross-section according to [49]; solid line: includes hard component according to [29] (as it is treated in this work).

τ -lepton energy losses in standard rock ($A=22$, $Z=11$) for photonuclear interaction and for the sum of all radiative processes are presented in Fig. 3. The importance of both corrections described above compared to the soft BB formula can be clearly seen. Results published in [49] for τ -lepton energy losses including another calculation of the hard component of the photonuclear cross-section are shown for comparison, as well. The main difference between [29] and [49] is due to the fact that corrections to the BB formula (soft part) [30,31] have not been introduced in [49]. The hard component of the photonuclear cross-section differs in [29] and [49], as well, since theoretical approaches applied in these two works are completely different.

2.3 Tau-lepton decay

To generate τ -lepton decays we used the TAUOLA package [67] which was developed for SLC/LEP experiments where τ -leptons are produced in e^+e^- collisions: $e^+e^- \rightarrow Z \rightarrow \tau^+\tau^-$. TAUOLA generates decays of τ^\pm 's of a given energy, taking into account all the effects of τ spin polarization. 22 decay modes are treated (sum to almost 100% of the total width) including modes that are responsible for ν_e and ν_μ appearance:

$$\tau^- \rightarrow e^- \bar{\nu}_e \nu_\tau \quad (\tau^+ \rightarrow e^+ \nu_e \bar{\nu}_\tau) \quad (4)$$

$$\tau^- \rightarrow \mu^- \bar{\nu}_\mu \nu_\tau \quad (\tau^+ \rightarrow \mu^+ \nu_\mu \bar{\nu}_\tau) \quad (5)$$

In our simulation we tracked only neutrinos (of all flavors) resulting from τ decay, since ranges of charged leptons are negligibly small compared to the Earth dimensions. Decay lengths of K 's and π 's resulting from τ decay are much longer than their interaction lengths in the considered energy range, hence we did not simulate their decay neglecting secondary neutrinos ³.

3 Results on ν_τ propagation through the Earth

In this section results on the simulation of propagation of ν_τ and $\bar{\nu}_\tau$ monoenergetic beams through the Earth are presented where all processes shown in Fig. 1 have been accounted for.

3.1 Results on monoenergetic tau-neutrino beams

The outgoing spectra of initially monoenergetic ν_τ 's after propagation through the Earth for three nadir angles of incidence on the Earth are shown in Fig. 4 for two neutrino energies: 10 TeV and 1 EeV. Moreover, the outgoing spectra of secondary ν_μ 's and ν_e 's that are produced in decays of τ -leptons generated in ν_τ CC interactions are presented. Results for ν_τ and $\bar{\nu}_\tau$ beams are identical. At $E_{\nu_\tau} = 10^4$ GeV neutrino cross-sections are small and most of τ -neutrinos cross the Earth without interacting keeping their initial energy (see the peaks in the upper panels in Fig. 4). The fraction of such neutrinos is lower at the nadir direction ($\theta = 0^\circ$) since the amount of matter crossed is maximum. This fraction increases with nadir angle. At $E_{\nu_\tau} = 10^9$ GeV all τ -neutrinos undergo at least one interaction and the peak at initial energy disappears

³ By the same reason we did not follow K 's and π 's produced in ν CC interactions.

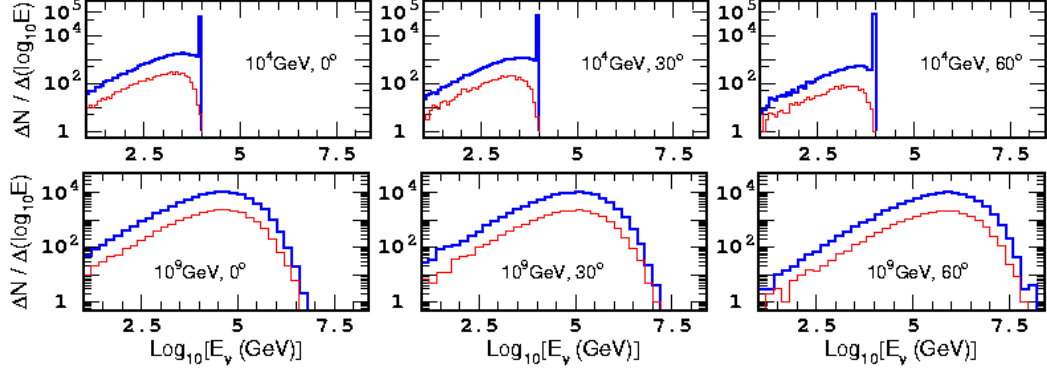


Fig. 4. Monoenergetic ν_τ beams incident on the Earth at nadir angles 0° (left), 30° (center), 60° (right). Results after propagation through the Earth. Upper row: $E_\nu^0 = 10$ TeV, lower row: $E_\nu^0 = 1$ EeV. Upper spectra: ν_τ ; lower spectra: secondary ν_μ ($= \nu_e$).

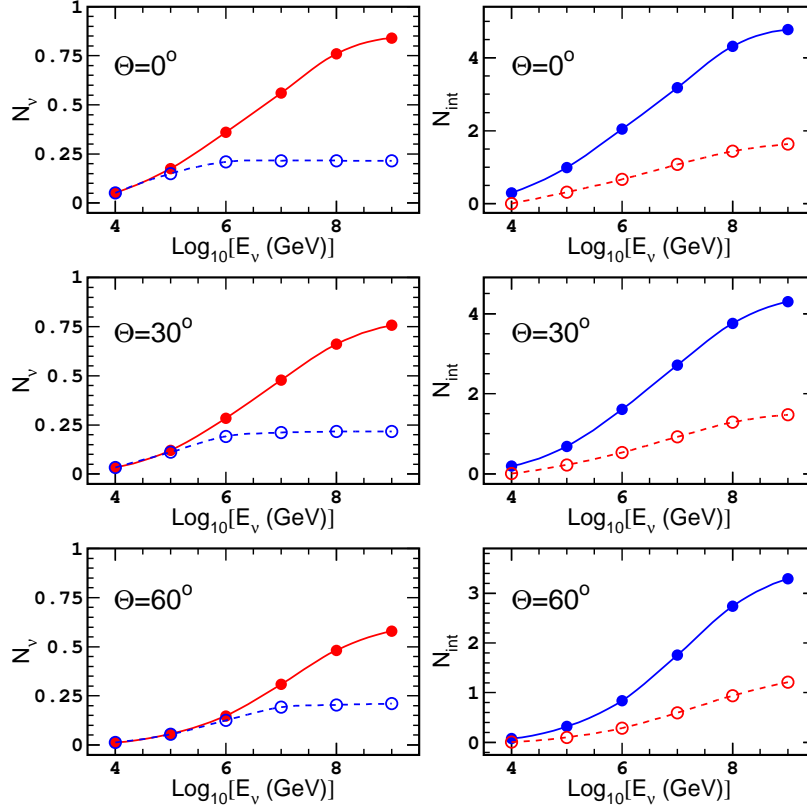


Fig. 5. Left column: Mean number of secondary ν_μ 's ($= \nu_e$'s) per ν_τ that are generated when a ν_τ crosses the Earth undergoing regeneration processes vs E_{ν_τ} (solid lines); mean number of secondary ν_μ 's ($= \nu_e$'s) that survive and come out from the Earth (dashed lines). Right column: mean number of CC (solid lines) and NC (dashed lines) interactions that occurs in the chain $\nu_\tau \rightarrow \tau \rightarrow \nu_\tau \dots$ when a τ -neutrino crosses the Earth vs its energy. Results for ν_τ and $\bar{\nu}_\tau$ are identical.

since neutrinos lose energy both in NC interactions and in regeneration chain. The fraction of secondary ν_e 's and ν_μ 's produced by the incoming ν_τ is 5%

at $E_{\nu_\tau} = 10^4$ GeV and 22% at $E_{\nu_\tau} = 10^9$ GeV for the nadir direction ⁴. These numbers are in good agreement with results published in [15].

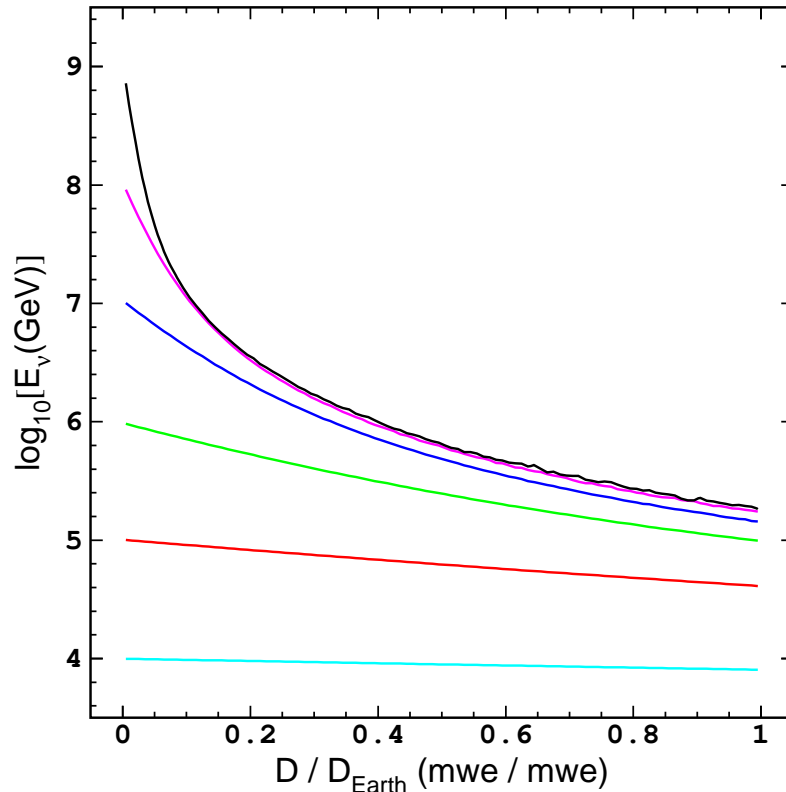


Fig. 6. Mean energy degradation for ν_τ with initial energies (from bottom to top): 10^4 GeV, 10^5 GeV, 10^6 GeV, 10^7 GeV, 10^8 GeV, 10^9 GeV when penetrating the Earth at nadir angle 0° vs fraction of Earth diameter crossed.

The fraction of secondary neutrinos that accompany τ -neutrinos emerging from the Earth increases with initial τ -neutrino energy but saturates at the level of 0.22 at some critical energy which depends upon nadir angle (Fig. 5, left column). These results are also in a good agreement with [15]. The CC cross-section increases with energy and, consequently, the number of secondaries generated along τ -neutrino path increases also. Nevertheless, this growth is moderated by absorption of secondary ν_μ 's and ν_e 's which, in contrast to ν_τ 's, do not regenerate. In the right column in Fig. 5 the mean number of NC and CC interactions occurring to a primary ν_τ ($\bar{\nu}_\tau$) when it travels through the Earth is shown. The number of CC interactions corresponds to the number of regeneration steps. This number grows both with τ -neutrino energy and with amount of matter crossed, which is maximum at the nadir.

Fig. 6 shows τ -neutrino energy losses due to regeneration process and NC interactions when crossing the Earth.

⁴ We consider all secondaries collinear with respect to the primary ν_τ , an approximation that at the energies to which we are interested is reasonable.

3.2 Results for some astrophysical diffuse ν spectra

We performed MC simulations for two spectra of cosmological neutrinos: the spectrum predicted by Protheroe [27] for an optically thick proton blazar model and an upper bound (not a source model) on diffuse ν spectrum for optically thick sources [28] (MPR bound) ⁵ (see Fig. 7).

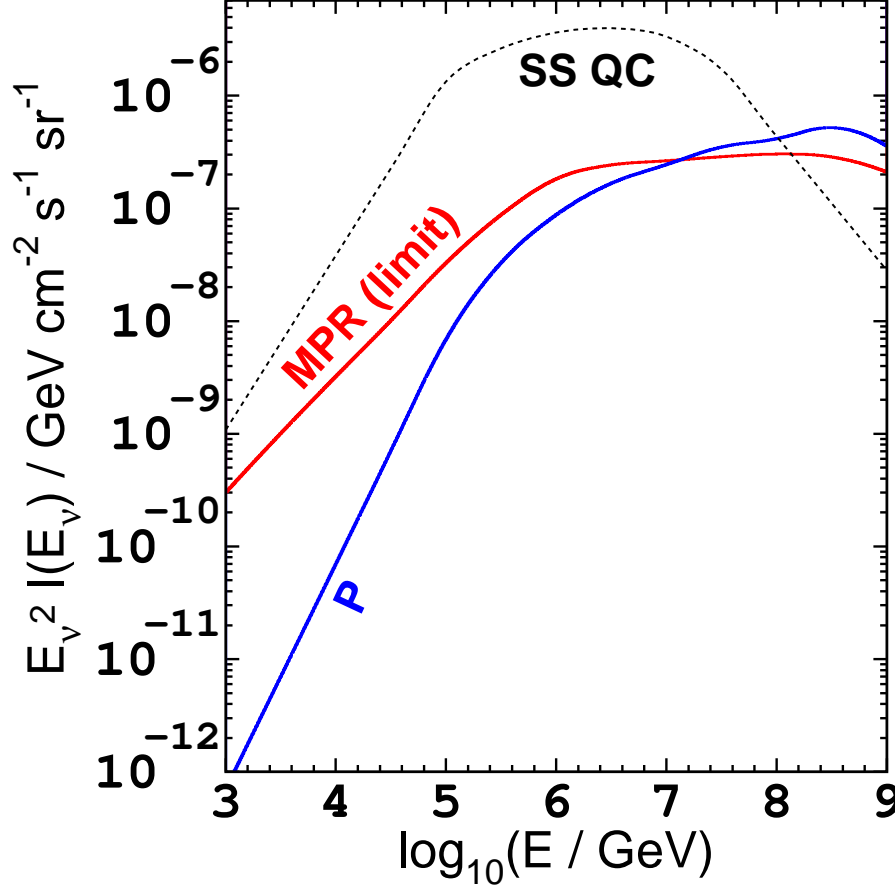


Fig. 7. Protheroe diffuse neutrino spectrum [27], MPR limit on diffuse neutrino spectrum [28] and 'Quasar background flux prediction' (SS QC) [68].

We have considered neutrinos of all flavors in the incoming flux including ν_e 's and ν_μ 's produced in sources and ν_τ 's that appear on the way to the Earth due to $\nu_\mu \leftrightarrow \nu_\tau$ oscillations. Neutrinos and anti-neutrinos of all flavors have been assumed to be present in the proportion $\phi_\nu : \phi_{\bar{\nu}} = 1 : 1$ in astrophysical neutrino fluxes. The background of $\nu_{\mu,e}$ atmospheric neutrinos from pion and kaon decays (conventional neutrinos), as well as the contribution of prompt ν 's from charmed mesons (calculated in the Recombination Quark-Parton Model

⁵ The 'Quasar background flux prediction' [68] was not considered, though it is more optimistic, since it is at the exclusion level by AMANDA [69,70] and Baikal [71] experiments.

frame) was simulated using spectra taken from [72].

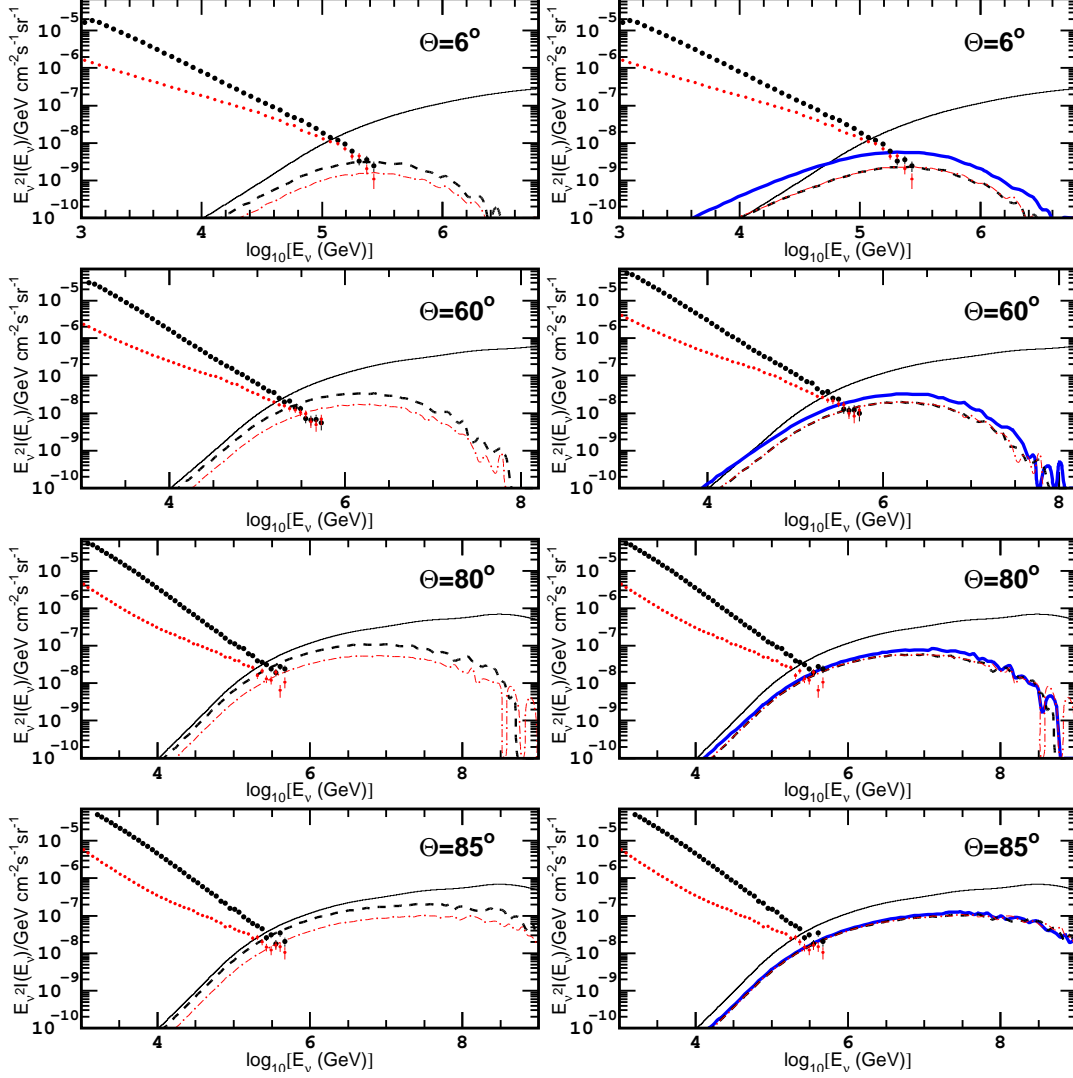


Fig. 8. Spectra of cosmological ν 's sampled according to Protheroe spectrum ([27]) incident on the Earth with 4 different nadir angles and after propagation through it. Left column: no oscillations, $\phi_{\nu_e}:\phi_{\nu_\mu}:\phi_{\nu_\tau} = 1:2:0$, right column: oscillations with maximal mixing, $\phi_{\nu_e}:\phi_{\nu_\mu}:\phi_{\nu_\tau} = 1:1:1$. Thin solid lines: total incoming flux of astrophysical ν 's; thick solid (right panels), dashed and dash-dotted lines (overlapping in right panels): out-coming $\nu_\tau + \bar{\nu}_\tau$, $\nu_\mu + \bar{\nu}_\mu$, $\nu_e + \bar{\nu}_e$ after propagation through the Earth, respectively. $\nu_{\mu,e}$ spectra include secondary neutrinos produced by ν_τ 's. In the left part of each panel atmospheric neutrino spectra (conventional+prompt [72]) after propagation through the Earth are shown, upper thick markers: $\nu_\mu + \bar{\nu}_\mu$, lower thin markers: $\nu_e + \bar{\nu}_e$. Atmospheric neutrino spectra are given up to ≈ 300 TeV where cosmological neutrino fluxes start to dominate since the simulation statistics at higher energies is very poor due to the steepness of spectra.

Results for Protheroe and MPR spectra for astrophysical neutrinos incident on the Earth with 4 different nadir angles and transformed after propagation through the Earth are shown in Fig. 8 and Fig. 9. τ -neutrino fluxes exceed $\nu_{\mu,e}$

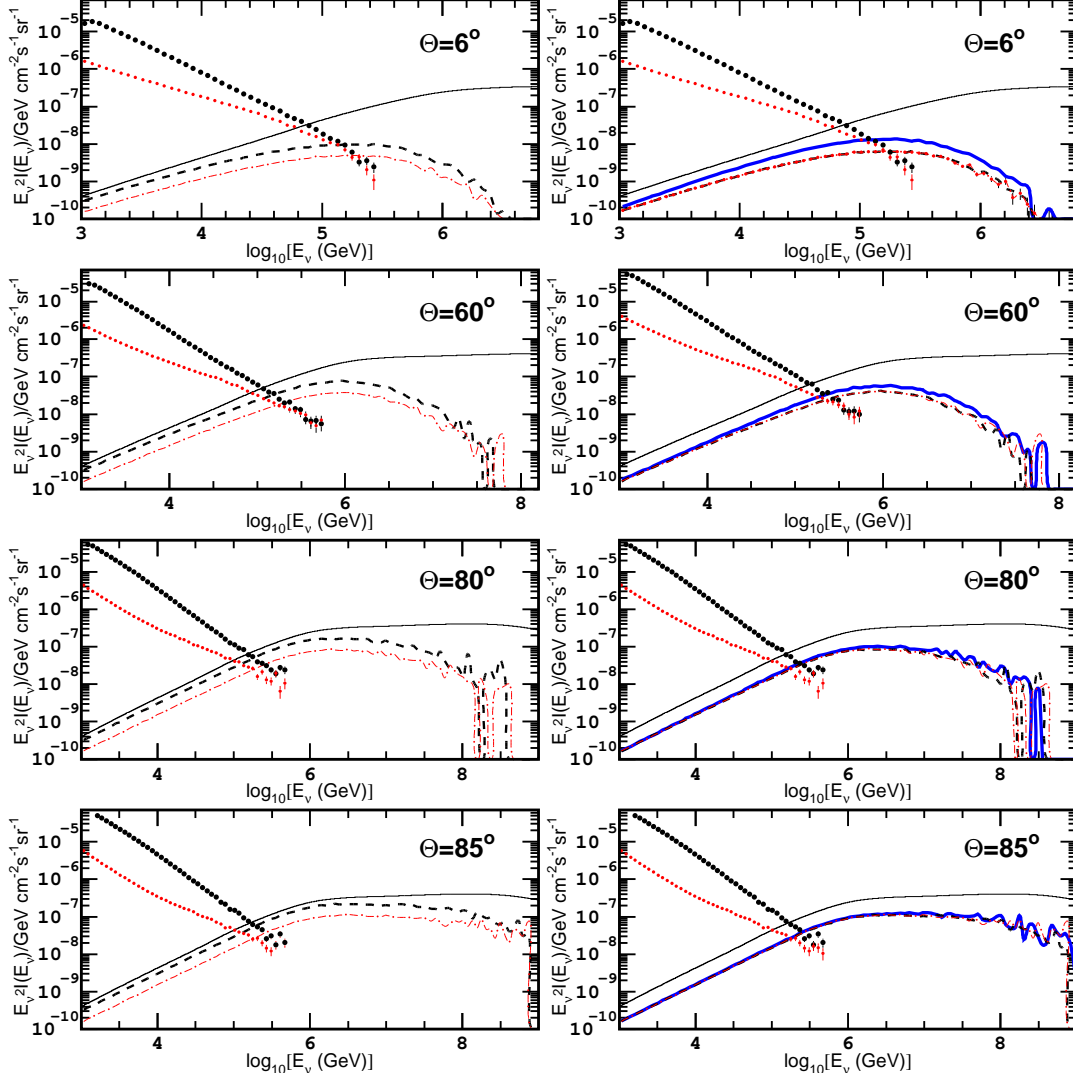


Fig. 9. The same as in Fig. 8 but astrophysical neutrinos are generated according to MPR upper limit on diffuse neutrino flux [28].

ones remarkably up to nadir angles $\theta \sim 60^\circ$ since ν_τ 's are not absorbed by the Earth in contrast to $\nu_{\mu,e}$'s. But their spectra are shifted to lower energies with respect to initial spectra due to energy degradation in regeneration processes. For all θ , the outgoing flux of astrophysical neutrinos exceeds the background of atmospheric neutrinos at $E_\nu \gtrsim 10^5$ GeV. This cross-over determines the energy threshold for detection of diffuse neutrino fluxes in UNTs. Results for Protheroe spectrum are in a qualitative agreement with ones published in [13] (see Fig.8 and Fig.9 there) where different models for neutrino interactions and τ -lepton energy losses were used. The fractions of secondary $\nu_{\mu,e}$'s produced in regeneration chains with respect to the total $\nu_{\mu,e}$ flux emerging after propagation through the Earth (made of of primary $\nu_{\mu,e}$'s + secondaries) are 0.57, 0.18, 0.06, 0.02 (spectrum [27]) and 0.18, 0.06, 0.02, 0.01 (spectrum [28]) for nadir angles $\theta = 6^\circ, 60^\circ, 80^\circ$, and 85° , respectively. These numbers

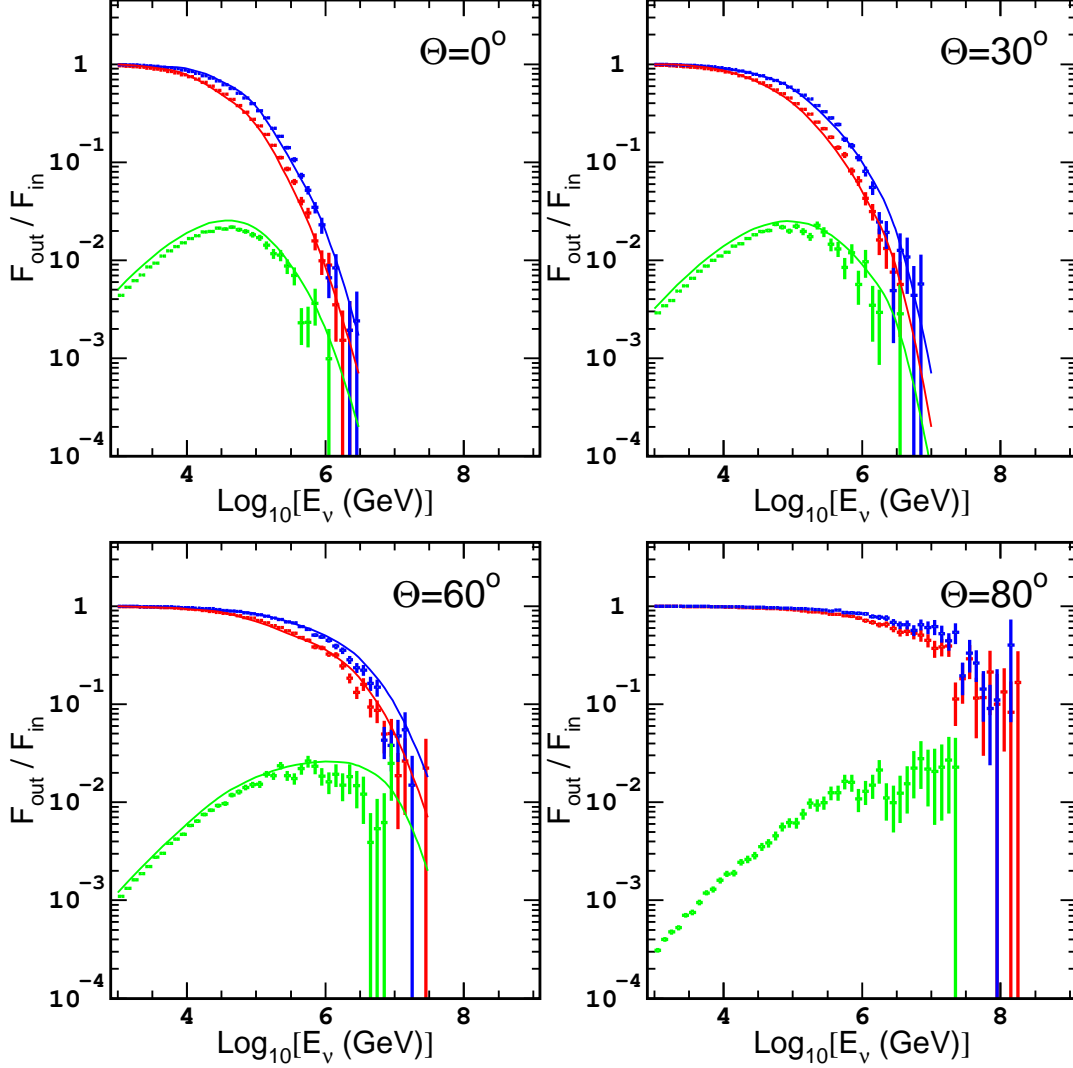


Fig. 10. The ratio of $\nu_\tau + \bar{\nu}_\tau$ (upper curves), $\nu_\mu + \bar{\nu}_\mu$ (middle curves) fluxes after propagation through the Earth and of secondary $\nu_\mu + \bar{\nu}_\mu (= \nu_e + \bar{\nu}_e)$ (lower curves) over incident flux $\propto E^{-2}$ for four nadir angles. Markers: this work, lines: results published in [16] for nadir angles $\theta=0^\circ$, $\theta=30^\circ$ and $\theta=60^\circ$ (data for $\theta=80^\circ$ are absent in [16]).

are larger than corresponding fractions for power-law spectra $\phi_\nu \propto E_\nu^{-1}$ and $\phi_\nu \propto E_\nu^{-2}$ reported in [16]⁶. On the other hand, the comparison of the results on attenuated neutrino fluxes obtained by our algorithm with the ones obtained in [16] for power-law spectra shows a reasonable agreement (Fig. 10). Hence, we can conclude that larger fractions of secondaries result from the fact that MPR and Protheroe spectra are harder compared to ones considered in [16].

⁶ Authors do not provide numbers, nevertheless one can estimate them from Fig. 1 in [16].

4 Tau leptons: detection signatures

4.1 Tau lepton identification through energy loss properties

At energies larger than $E_\tau \approx 2 \cdot 10^6$ GeV τ -lepton ranges become comparable to the typical linear dimensions of operating and proposed UNTs (see Fig. 11) and τ tracks can be reconstructed. As a first guess, one could try to distinguish a τ -lepton track from a muon one by means of differences in energy losses. The larger τ mass affects bremsstrahlung, e^+e^- -pair production and photonuclear processes differently respect to muons. As a result, e^+e^- -pair production dominates muon energy losses up to $E_\mu \approx 10^8$ GeV while τ -lepton photonuclear interaction plays the main role above $E_\tau \approx 10^5$ GeV (see Fig. 12) compared to other radiative processes. Hence, since probabilities of shower production for muons and τ -leptons at a given energy are different, one could hope to select τ -lepton events studying the distribution of showers produced in photonuclear or electromagnetic interactions along tracks even if the detector resolution is not so good to discriminate hadronic and electromagnetic showers.

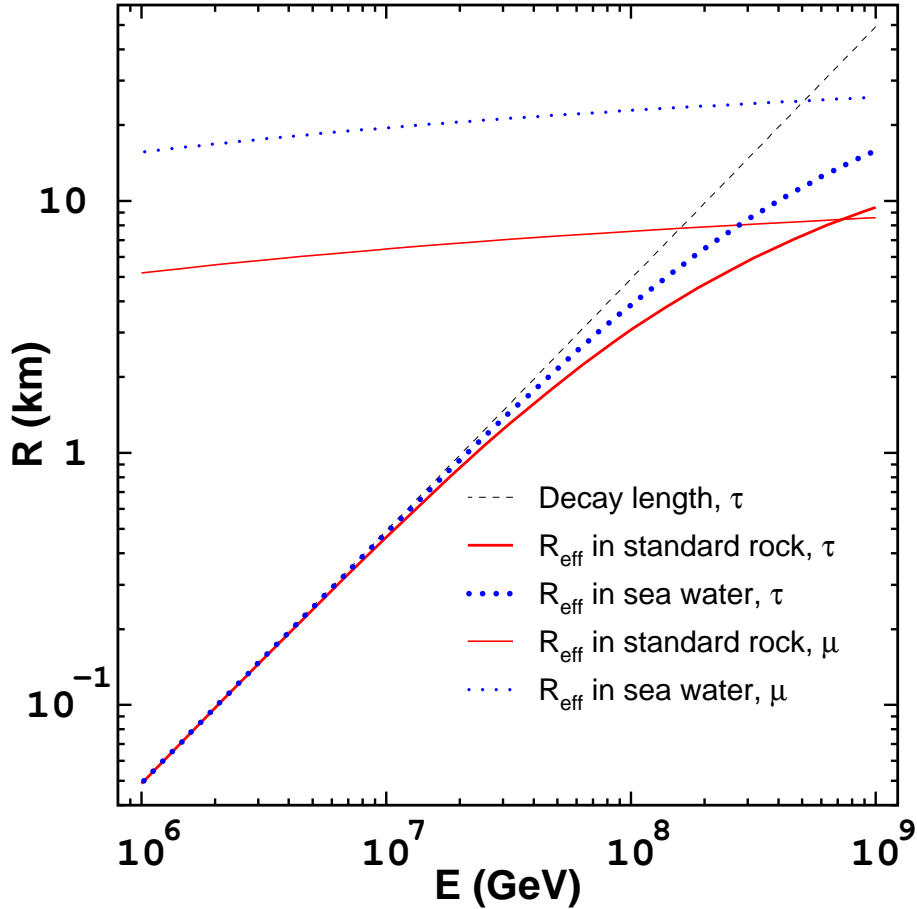


Fig. 11. Mean ranges for muons and τ -leptons in standard rock and sea water.

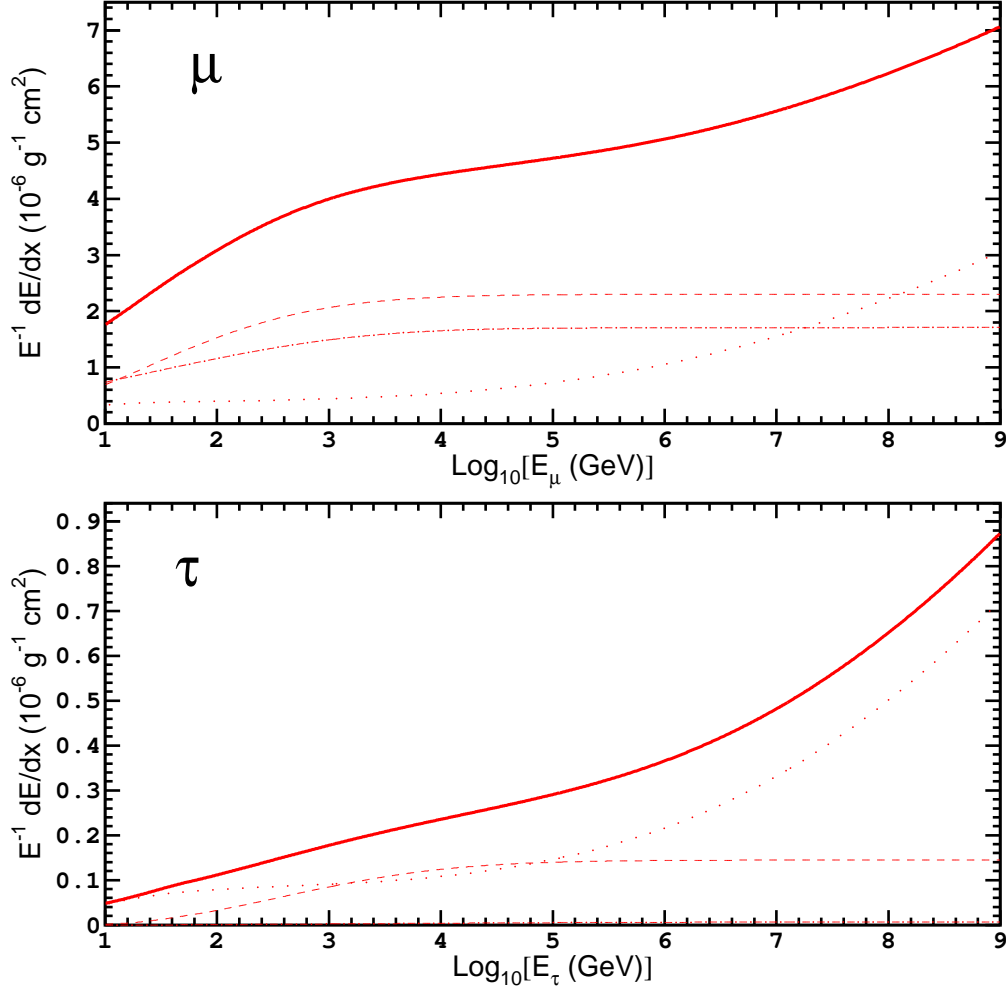


Fig. 12. Muon (upper plot) and τ -lepton (lower plot) energy losses in standard rock due to bremsstrahlung (dash-dotted lines), direct e^+e^- -pair production (dashed lines), photonuclear interaction (dotted lines). Thick solid lines stand for total radiative energy losses. Bremsstrahlung for τ -lepton is strongly suppressed due to m^{-2} factor, therefore the bremsstrahlung curve almost coincides with the x -axis.

Nevertheless, the results of the calculation that we have performed for τ -leptons with energies in the range $10^6 \text{ GeV} \leq E_\tau \leq 10^9 \text{ GeV}$ indicate that such a method works badly because the largest differences between shapes of τ -lepton and muon cross-sections lies in a range of relatively large $v = \Delta E/E$, where interaction lengths exceed the detector size. The numerical data on τ -leptons of energies 10^7 GeV and 10^9 GeV and muons of lower energies ($1.10 \cdot 10^6$ and $1.56 \cdot 10^8$, respectively) are presented in Fig. 13 and Fig. 14, which show values of energy losses and radiation lengths for different ranges of energy transferred to secondaries ($10^0 \text{ GeV} \leq \Delta E \leq 10^1 \text{ GeV}$, $10^1 \text{ GeV} \leq \Delta E \leq 10^2 \text{ GeV}$, ..., $10^6 \text{ GeV} \leq \Delta E \leq 10^7 \text{ GeV}$). Muon energies were chosen so that total muon energy losses are equal to total energy losses of considered τ -leptons. Data on electromagnetic processes (bremsstrahlung + e^+e^- -pair production), photonuclear interaction and all interactions are presented separately. One can

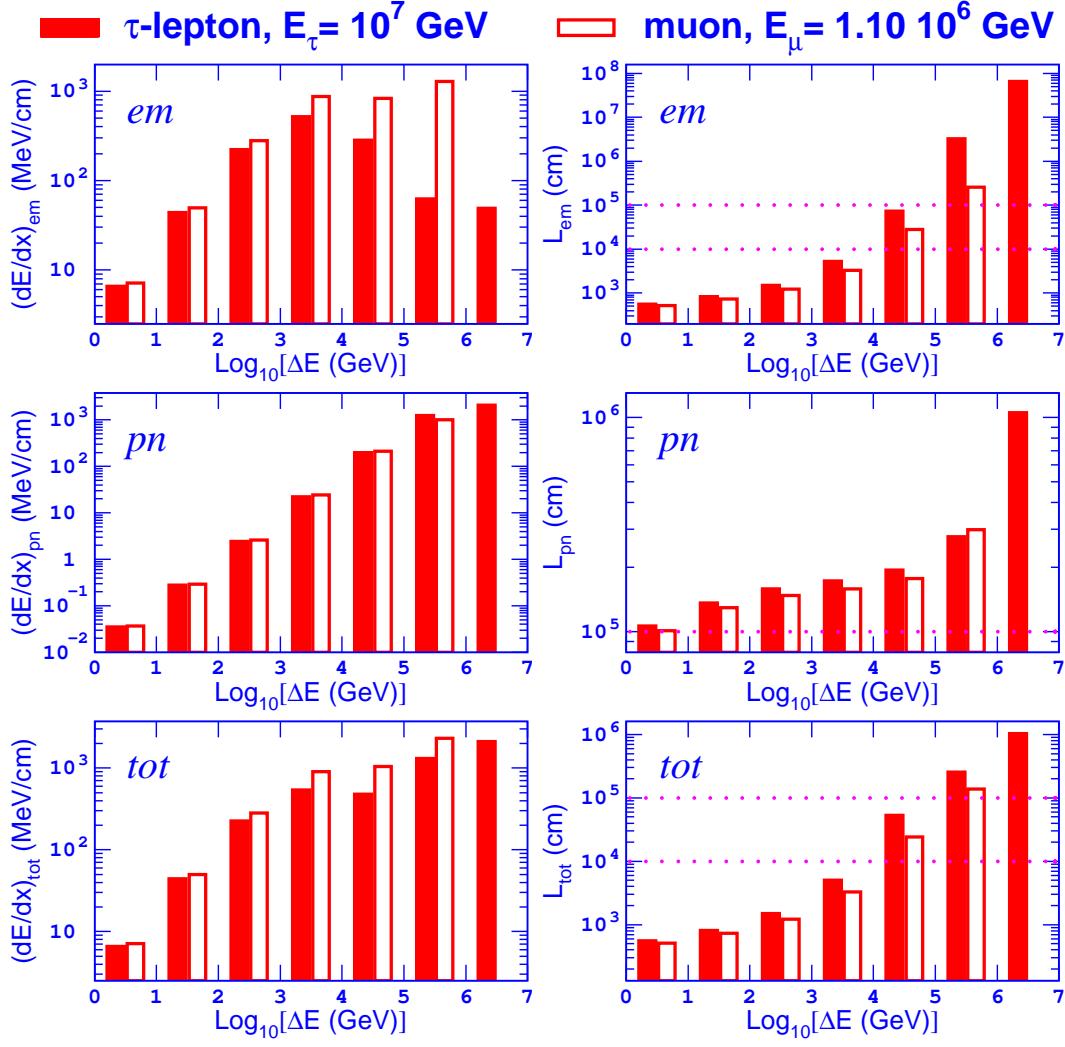


Fig. 13. Left column: energy losses in sea water due to electromagnetic interactions (upper panel), photonuclear interactions (middle panel) and all interactions (lower panel) for energy transferred to secondaries belonging to different ranges ($10^0 \text{ GeV} \leq \Delta E \leq 10^1 \text{ GeV}$, $10^1 \text{ GeV} \leq \Delta E \leq 10^2 \text{ GeV}$, ..., $10^6 \text{ GeV} \leq \Delta E \leq 10^7 \text{ GeV}$). Filled boxes correspond to a τ -lepton with $E_\tau = 10^7$ GeV, empty ones to a muon with energy $E_\mu = 1.1 \cdot 10^6$ GeV. Right column: Mean interaction length of muon/ τ -lepton in sea water for different ranges of energy transferred to secondaries. The horizontal lines indicate 100 m and 1 km which are the typical linear sizes of existing and planned UNTs.

see that 'partial' energy losses and radiation lengths of τ -leptons and muons of lower energies differ remarkably only for large transferred energies when radiation length exceeds 100 - 1000 m, typical linear dimensions of existing and planned detectors. Thus, there are too few high energy showers inside the detector sensitive volume to provide enough statistics to distinguish τ -lepton and muon tracks. Even in the hypothesis that the detector capability is so good to distinguish electromagnetic showers from hadronic ones, it is very

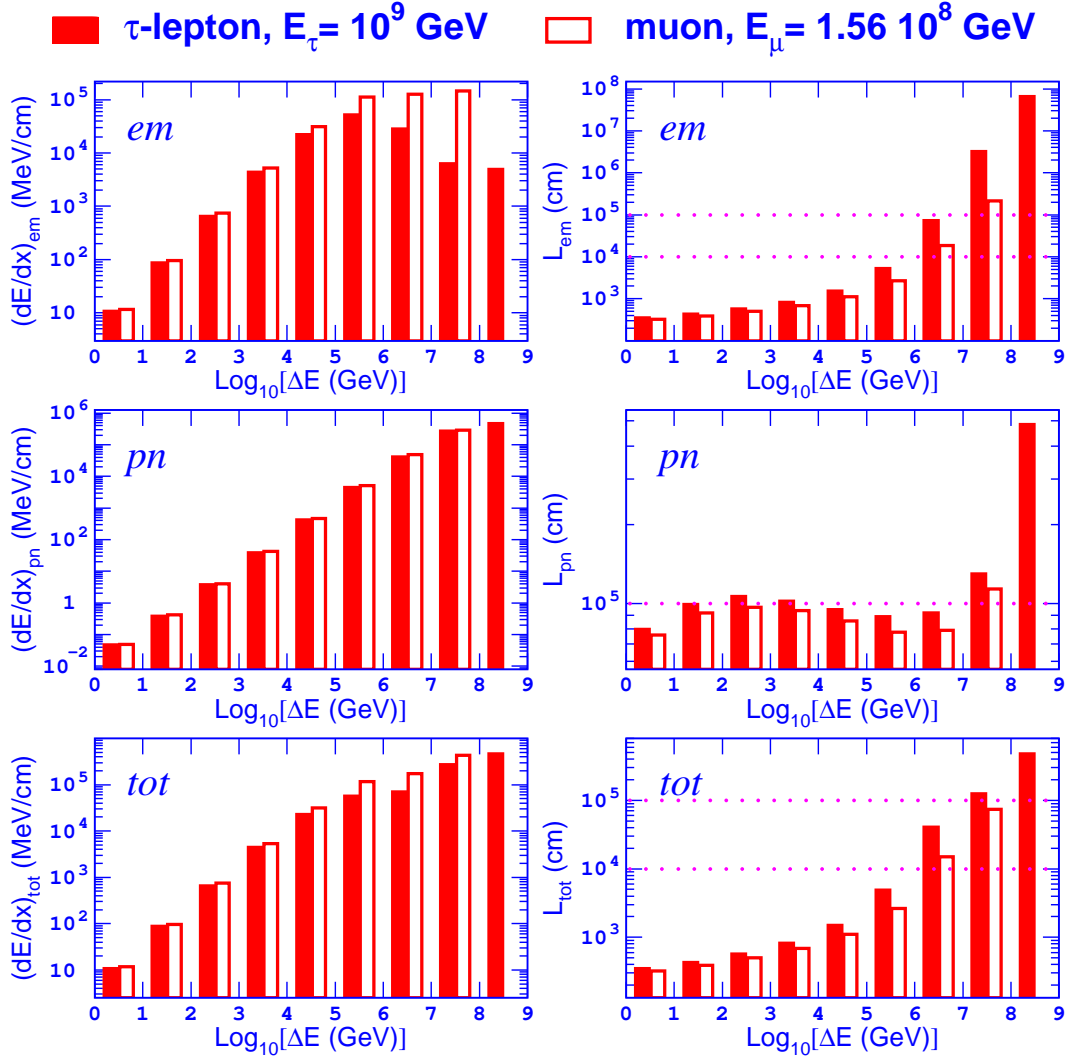


Fig. 14. The same as in Fig. 13 for a 10^9 GeV τ -lepton and a $1.56 \cdot 10^8$ GeV muon.

difficult and, most probably, impossible to distinguish a τ -lepton track of a certain energy with respect to a muon track of $\sim 6 \div 11$ times lower energy. This difficulty also concerns 1 km^3 -scale UNTs. Of course, the observation of a very high energy shower with reconstructed energy so large to be inconsistent with the energy reconstructed using the rest of the track could be an indication in favor of a τ -lepton. Nevertheless, the probability of such a shower occurrence is too small that this cannot be considered a standard reliable method.

4.2 Topological signatures

As a matter of fact, signatures such as 'double bang' (DB) or 'lollipop' events proposed in [21] seem to be smoking guns to recognize τ -lepton events in UNTs. DB event features are an hadronic cascade at the νN CC interaction

vertex and an hadronic or electromagnetic cascade corresponding to τ -lepton decay. The τ -lepton track connects both cascades⁷. A lollipop event consists of a partially contained τ -lepton track with the first cascade at the ν interaction vertex outside of the UNT sensitive volume and with the second cascade produced by τ -lepton decay contained in the volume. On the other hand, the inverse pattern with only the first cascade visible can not be distinguished from $\nu_\mu N \rightarrow \mu N$ interaction followed by the muon track. Both DB and lollipop signatures provide a clear and background-free evidence of ν_τ detection. As a matter of fact, for τ decaying into electronic and hadronic channels there is no muon track following the second cascade. Besides, DB events do not contain an in-coming track before the first cascade. In principle, an up-going muon generated in a ν_μ CC interaction could mimic such a signature if it would produce a shower that takes all the muon energy inside the instrumented volume. But the probability to have such an event for a muon track segment of the order of 1 km is less than $5 \cdot 10^{-4}$ in water for energies larger than 1 PeV. This value corresponds to the probability that a muon loses more than 99% of its energy in one interaction. This number can be considered as an upper limit on the signal to noise ratio, where the signal are DB/lollipop events and the noise are up-going ν -induced muons. In fact, astrophysical ν_μ fluxes are lower or at most equal to expected astrophysical ν_τ ones after propagation in the Earth and atmospheric neutrino fluxes are even lower above 1 PeV (see Fig. 8 and Fig. 9). Another background source could be due to atmospheric muons that are dominated by prompt muons in the considered energy range. DB events cannot be reproduced since in any case the muon track before the first cascade would be visible. Nevertheless, a muon can mimic a lollipop event if it enters the detector instrumented volume and undergoes an interaction with such a large energy transfer that the muon stops after shower production. We estimate a rate of $\sim 50 \text{ km}^{-3} \text{ yr}^{-1}$ considering the probability upper limit of $5 \cdot 10^{-4}$ (corresponding to more than 99% muon energy loss) and the prompt muon fluxes published in [73,74]. However, this is an upper limit since it is not possible to compute exactly the probability that a muon loses 100% of its energy since cross section parameterizations close to $v = \Delta E/E = 1$ do not describe perfectly well the real cross sections. Of course more quantitative conclusions on possible backgrounds are needed that should be based on detailed simulations including detector response and

⁷ One should note that at energies where the τ -lepton track connecting the 2 cascades can be reconstructed in a UNT ($E_\tau \gtrsim 1 \text{ PeV}$), the τ is not a minimum ionizing track, as instead it is assumed in [21]. In the example considered in [21] (a 1.8 PeV τ -lepton) about $5.5 \cdot 10^8$ Čerenkov photons in the wavelength range $350 \text{ nm} \leq \lambda \leq 600 \text{ nm}$ are emitted by a 90 m long track. This number is ~ 300 times larger than for a minimum ionizing track. Nonetheless it is still several orders of magnitude lower than the number of photons from both cascades ($\approx 4 \cdot 10^{11}$ and $\approx 10^{11}$ from first and second cascades, respectively), thus the signature of DB remains unchanged with this correction.

reconstruction algorithms. At least qualitatively, DB and lollipop events are potentially “background free”, as it has been stated in the paper that proposed the existence of these topologies [21].

In 17% of the cases, that is for the τ decay channel into a muon (see eq. 5), the second cascade is absent. In this case the τ -lepton track is followed by a muon track without any shower. This topology seems to be not-recognizable as a τ -lepton signature in a UNT, although the amount of light produced by showers along the τ track (hereafter ‘brightness’) differs essentially from that along a muon track of the same energy. As an example, let us consider a τ -lepton of energy $E_\tau = 10^7$ GeV that decays into a muon. For a simple estimation, we assume that the muon takes 1/3 of the τ energy, thus $E_\mu \approx 3.3 \cdot 10^6$ GeV. From results in Sec. 4.1 (see Fig. 13) we know that the brightness of a 10^7 GeV τ track is similar to that of a μ track with $E_\mu = 1.1 \cdot 10^6$ GeV. After τ -lepton decay, the track brightness increases by about a factor of $\approx 3.3 \cdot 10^6 \text{ GeV} / 1.1 \cdot 10^6 \text{ GeV} = 3$. This factor depends on τ -lepton energy and in the range $10^6 \text{ GeV} \leq E_\tau \leq 10^9 \text{ GeV}$ it varies between 2 and 4. To recognize such a signature detector energy reconstruction should be remarkably better than this factor, which is not always the case for neutrino telescopes (see for instance Fig. 4 from [75]). Thus, when computing DB or/and lollipop event rates in a UNT, results must be reduced by a factor $B_{-\mu} = 0.83$ to exclude the non-muonic branching ratio in τ -lepton decay.

Estimates of DB rates in km^3 UNTs have already been presented in [22] for down-going ν_τ ’s, while events from the lower hemisphere were not considered. Calculations of up-going ν_τ propagation were done in [14]. Authors give a qualitative conclusion that though UHE/EHE ν_τ ’s are not absorbed by the Earth, their energies decrease; hence the expected amount of τ events in the DB energy range is low. Calculations in [24] performed for a neutrino flux $E_{\nu_\mu}^2 dN_{\nu_\mu} / dE_{\nu_\mu} = 10^{-7} \text{ GeV cm}^{-2} \text{ s}^{-1}$ assuming ν oscillations but without accounting for neutrino absorption in the Earth result in a rate of $\approx 0.5 \text{ yr}^{-1}$ both for DB and lollipop events in an IceCube-like km^3 detector [4]. The measurement of the ratio between muon and shower events that may be an indirect signature of ν_τ appearance was proposed in [14,24] as an alternative indirect way to detect τ -neutrinos. Here we present results of a calculation of the DB rate for both the upper and lower hemispheres in a km^3 scale UNTs using results reported in Sec. 3 for the spectra in [27,28] that were not considered in [14,22,24]. The rate of totally contained DB events in a UNT is given by:

$$n_{DB} = 2\pi \rho N_A B_{-\mu} \int_{-1E_{min}}^{0(1)} \int_0^\infty V_{eff}(E_{\nu_\tau}, \theta) I(E_{\nu_\tau}, \theta) \sigma^{CC}(E_{\nu_\tau}) dE_{\nu_\tau} d(\cos \theta) \quad (6)$$

Here N_A is the Avogadro number, ρ is the medium density (we use $\rho = 1 \text{ g cm}^{-3}$ which is close to sea water/ice density), $I(E_{\nu_\tau}, \theta)$ is the differential ν_τ flux. The

Earth shadowing effect is accounted for in the case of the lower hemisphere (for which the upper limit of the integral is 0, while $\cos \theta = 1$ is used to compute the number of events for the whole sphere). The effective volume is:

$$V_{eff} = S_p(\theta) (L - R_\tau(E_{\nu_\tau})), \quad (7)$$

where S_p is the projected area for tracks generated isotropically in azimuth for a fixed θ direction of the incident neutrino on a parallelepiped. The parallelepiped has the dimensions of an IceCube-like detector [4] ($1 \times 1 \times 1 \text{ km}^3$) or a NEMO-like one [5] ($1.4 \times 1.4 \times 0.6 \text{ km}^3$). In eq. 7, L is the geometrical distance between entry and exit point from the parallelepiped, R_τ is the τ -lepton range, σ^{CC} is total CC ν cross-section. $E_{min} = 2 \cdot 10^6 \text{ GeV}$ corresponds to a τ -lepton range of $R_\tau^{min} = 70 \text{ m}$.

Table 1

Number of DB events in km^3 detector per year.

Spectrum	IceCube-like ($N_{-2\pi} / N_{2\pi} / N_{4\pi}$)	NEMO-like ($N_{-2\pi} / N_{2\pi} / N_{4\pi}$)
<i>Protheroe</i>	0.6 / 1.3 / 1.9	0.8 / 1.7 / 2.5
<i>MPR</i>	0.8 / 1.9 / 2.7	1.2 / 2.6 / 3.8

Table 1 shows DB rates for the lower, upper and for both hemispheres. Values for upper hemisphere are $3 \div 6$ times lower compared to [22] since more optimistic predictions for diffuse neutrino fluxes [68] are used there. At the same time, our figures for DB rates in IceCube-like UNT are $4 \div 5$ higher compared to results reported in [24]. There are at least four factors that contribute to this difference:

- different ν flux models are used;
- minimum τ range is $R_\tau^{min} = 70 \text{ m}$ in our calculations while in [24] it is equal to $R_\tau^{min} = 200 \div 400 \text{ m}$. Such a large minimum range was chosen according to the qualitative requirement to reconstruct the τ -lepton track connecting the two cascades. This difference accounts for a factor of ~ 4 in the case of an E^{-2} ν flux between 10^6 and 10^7 GeV . Since horizontal photomultiplier spacing in IceCube detector is $\sim 125 \text{ m}$, but the vertical spacing is 17 m [4], we believe that this requirement could be too restrictive. The proper choice of the minimum range should indeed be done quantitatively using a full simulation of the detector including reconstruction procedures;
- for the lower hemisphere we accounted for τ -neutrino energy losses in the Earth. This losses can be such that events do not fall anymore above the DB ‘energy threshold’ (that figures for lower hemisphere in Table 1 are about a factor of ≈ 2 lower compared to the upper hemisphere ones). These losses were not accounted for in [24];
- in contrast to [24] we reduce all figures for rates by a factor $B_{-\mu} = 0.83$ to exclude the muonic mode of τ -lepton decay.

5 Conclusions

Considering the AGN diffuse neutrino flux models in [27] and the upper limit on optically thick ν sources in [28] we have found that in a km^3 UNT one can expect $2\div 4$ DB events yr^{-1} ⁸. This result depends on the assumed neutrino spectrum and on the minimum τ -lepton range that can be reconstructed in the detector, hence on its geometry and reconstruction algorithms. Hence, these values should be considered as indicative, while full simulations for specific neutrino telescopes should be performed. Moreover, we have investigated the possibility of identification of τ -lepton from muons by studying the distribution of showers produced by electromagnetic and photonuclear interactions along the track. This seems to be very difficult. Detection of DB or lollipop events are the cleanest signatures even though rates seem to be quite small. An alternative indirect way to identify τ 's consists in measuring the ratio between shower and track events. In any case, simulations of τ -neutrino propagation through the Earth should be performed including regeneration processes and τ -lepton energy losses. For this, in particular, one needs to account for corrections to the soft part of the photonuclear interaction which increases the total τ -lepton energy losses by $\approx 20\div 30\%$ in UHE/EHE range.

Acknowledgments

We thank P. Lipari for providing the original ν cross-section generator.

A Appendix: photonuclear cross-section

The differential cross-section for photonuclear interaction used in this work has been published in [29]. It is rewritten below in the form adopted in [43] (Appendix A). In the formula the following values are used: $\alpha = 7.297353 \times 10^{-3}$ – fine structure constant; $A \equiv$ atomic weight; $m_l = m_\mu = 0.1057 \text{ GeV}$ for muon and $m_l = m_\tau = 1.777 \text{ GeV}$ for τ -lepton; $m_N \equiv$ nucleon mass; $\pi = 3.141593$.

⁸ The rate of lollipop events is expected to be slightly larger than that of DB events. In fact, for lollipops the second cascade is not required to be inside an UNT, while for DB both should be contained. Hence, the detection probability for lollipop events is essentially larger than for DB at $E_\tau \gtrsim 10 \text{ PeV}$ [24], but due to the steepness of neutrino spectra the difference in rates is not very large. Nevertheless, an estimate would require a more detailed detector simulation than what has been done in this work.

Table A.1

Coefficients a_k for $\frac{d\sigma_{hard}^{pn}}{dv} = \frac{1}{v} \sum_{k=0}^7 a_k \log_{10}^k v$ in the formula for photonuclear cross-section. The upper figures stand for muons, lower ones does for τ -leptons.

E (GeV)	a_0	a_1	a_2	a_3
10^3	7.174409 $\cdot 10^{-4}$ -1.269205 $\cdot 10^{-4}$	-0.2436045 -0.01563032	-0.2942209 0.04693954	-0.1658391 0.05338546
10^4	1.7132 $\cdot 10^{-3}$ -2.843877 $\cdot 10^{-4}$	-0.5756682 -0.03589573	-0.68615 0.1162945	-0.3825223 0.130975
10^5	4.082304 $\cdot 10^{-3}$ -5.761546 $\cdot 10^{-4}$	-1.553973 -0.07768545	-2.004218 0.3064255	-1.207777 0.3410341
10^6	8.628455 $\cdot 10^{-3}$ -1.195445 $\cdot 10^{-3}$	-3.251305 -0.157375	-3.999623 0.7041273	-2.33175 0.7529364
10^7	0.01244159 -1.317386 $\cdot 10^{-3}$	-5.976818 -0.2720009	-6.855045 1.440518	-3.88775 1.425927
10^8	0.02204591 -9.689228 $\cdot 10^{-15}$	-9.495636 -0.4186136	-10.05705 2.533355	-5.636636 2.284968
10^9	0.03228755 -6.4595 $\cdot 10^{-15}$	-13.92918 -0.8045046	-14.37232 3.217832	-8.418409 2.5487
E (GeV)	a_4	a_5	a_6	a_7
10^3	-0.05227727 0.02240132	-9.328318 $\cdot 10^{-3}$ 4.658909 $\cdot 10^{-3}$	-8.751909 $\cdot 10^{-4}$ 4.822364 $\cdot 10^{-4}$	-3.343145 $\cdot 10^{-5}$ 1.9837 $\cdot 10^{-5}$
10^4	-0.1196482 0.05496	-0.02124577 0.01146659	-1.987841 $\cdot 10^{-3}$ 1.193018 $\cdot 10^{-3}$	-7.584046 $\cdot 10^{-5}$ 4.940182 $\cdot 10^{-5}$
10^5	-0.4033373 0.144945	-0.07555636 0.03090286	-7.399682 $\cdot 10^{-3}$ 3.302773 $\cdot 10^{-3}$	-2.943396 $\cdot 10^{-4}$ 1.409573 $\cdot 10^{-4}$
10^6	-0.7614046 0.3119032	-0.1402496 0.06514455	-0.01354059 6.843364 $\cdot 10^{-3}$	-5.3155 $\cdot 10^{-4}$ 2.877909 $\cdot 10^{-4}$
10^7	-1.270677 0.5576727	-0.2370768 0.1109868	-0.02325118 0.011191	-9.265136 $\cdot 10^{-4}$ 4.544877 $\cdot 10^{-4}$
10^8	-1.883845 0.8360727	-0.3614146 0.1589677	-0.03629659 0.015614	-1.473118 $\cdot 10^{-3}$ 6.280818 $\cdot 10^{-4}$
10^9	-2.948277 0.8085682	-0.5819409 0.1344223	-0.059275 0.01173827	-2.419946 $\cdot 10^{-3}$ 4.281932 $\cdot 10^{-4}$

$$\begin{aligned}
\frac{d\sigma_{pn}}{dv} = & \frac{\alpha}{8\pi} A \sigma_{\gamma N} v \left\{ \left(H(v) + \frac{2m_l^2}{m_2^2} \right) \ln \left(1 + \frac{m_2^2}{t} \right) \right. \\
& - \frac{2m_l^2}{t} \left[1 - \frac{0.25m_2^2}{t} \ln \left(1 + \frac{t}{m_2^2} \right) \right] + G(z) \left[H(v) \left(\ln \left(1 + \frac{m_1^2}{t} \right) - \frac{m_1^2}{m_1^2+t} \right) \right. \\
& \left. \left. + \frac{4m_l^2}{m_1^2} \ln \left(1 + \frac{m_1^2}{t} \right) - \frac{2m_l^2}{t} \left(1 - \frac{0.25m_1^2-t}{m_1^2+t} \right) \right] \right\} + A \frac{d\sigma_{hard}^{pn}}{dv},
\end{aligned}$$

$$H(v) = 1 - \frac{2}{v} + \frac{2}{v^2},$$

$$G(z) = \frac{9}{z} \left[\frac{1}{2} + \frac{(1+z)e^{-z} - 1}{z^2} \right] \quad (Z \neq 1),$$

$$G(z) = 3 \quad (Z = 1),$$

$$z = 0.00282 A^{1/3} \sigma_{\gamma N}, \quad t = \frac{m_l^2 v^2}{1-v}, \quad m_1^2 = 0.54 \text{ GeV}^2, \quad m_2^2 = 1.80 \text{ GeV}^2$$

with total cross-section for absorption of a real photon of energy $\nu = s/2m_N = vE$ by a nucleon, $\sigma_{\gamma N}$, parameterized according to [30,31]

$$\sigma_{\gamma N} = [114.3 + 1.647 \ln^2(0.0213 \nu)] \mu b$$

and hard part of cross-section described by polynomial parameterization

$$\frac{d\sigma_{hard}^{pn}}{dv} = \frac{1}{v} \sum_{k=0}^7 a_k \log_{10}^k v$$

(coefficients a_k are given in Table A.1). Parameterization for $\frac{d\sigma_{hard}^{pn}}{dv}$ is valid in the range $10^{-6} \leq v \leq 1$, $10^3 \leq E \leq 10^9 \text{ GeV}$, in MUM 1.5 $\frac{d\sigma_{hard}^{pn}}{dv}$ is assigned to 0 for $E = 10^2 \text{ GeV}$ and $v = 10^{-7}$, values between $v = 10^{-7}$ and $v = 10^{-6}$, as well as between $E = 10^2 \text{ GeV}$ and $E = 10^3 \text{ GeV}$ are computed by interpolation. Values for energies between ones that are given in the Table A.1 are computed by interpolation, as well.

References

- [1] AMANDA Collaboration: P. Desiati et al., astro-ph/0306536; see URL <<http://amanda.uci.edu/>>.
- [2] ANTARES Collaboration: E. Aslanides et al., astro-ph/9907432; T. Montaruli et al., in: Proceedings of 28th International Cosmic Ray Conference, Tsukuba, 2003, p.1357. Available from <arXiv:physics/0306057>; see URL <<http://antares.in2p3.fr/>>.
- [3] Baikal Collaboration: R. Wischnewski et al., in: Proceedings of 28th International Cosmic Ray Conference, Tsukuba, 2003. Available from <arXiv:astro-ph/0305302>; see URL <<http://nt200.da.ru/>>.
- [4] IceCube Collaboration: J. Ahrens et al., astro-ph/0305196; see URL <<http://icecube.wisc.edu/>>.
- [5] NEMO Collaboration: G. Riccobene et al., in: Proceedings of second Workshop on Methodical Aspects of Underwater/Underice Neutrino Telescopes, Hamburg, 2001, p. 61; see URL <<http://nemoweb.lns.infn.it/>>.
- [6] NESTOR Collaboration: S. E. Tzamarias et al., NIM A502 (2003) 150; see URL <<http://www.nestor.org.gr/>>.
- [7] Super-Kamiokande Collaboration: S. Fukuda et al., Phys. Rev. Lett. 85 (2000) 3999. Available from <arXiv:hep-ex/0009001>.
- [8] MACRO Collaboration: M. Ambrosio et al., Phys. Lett. B517 (2001) 59. Available from <arXiv:hep-ex/0106049>.
- [9] K2K Collaboration: M. H. Ahn et al., Phys. Rev. Lett. 90 (2003) 041801. Available from <arXiv:hep-ex/0212007>.
- [10] G. Barenboin, C. Quigg, Phys. Rev. D67 (2003) 073024. Available from <arXiv:hep-ph/0301220>.
- [11] J. F. Beacom, Phys. Rev. Lett. 90 (2003) 181301. Available from <arXiv:hep-ph/0211305>.
- [12] Particle Data Group: K. Hagiwara et al., Phys. Rev. D66 (2002) 010001. Available from <<http://pdg.lbl.gov/>>.
- [13] J. Kwiecinski, A. D. Martin, A. M. Stasto, Phys. Rev. D59 (1999) 093002. Available from <arXiv:astro-ph/9812262>.
- [14] S. I. Dutta, M. H. Reno, I. Sarcevic, Phys. Rev. D62 (2000) 123001. Available from <arXiv:hep-ph/0005310>.
- [15] J. F. Beacom, P. Crotty, E. W. Kolb, Phys. Rev. D66 (2002) 021302(R). Available from <arXiv:astro-ph/0111482>.
- [16] S. I. Dutta, M. H. Reno, I. Sarcevic, Phys. Rev. D66 (2002) 077302. Available from <arXiv:hep-ph/0207344>.

- [17] S. Yoshida, R. Ishibashi, H. Miyamoto, astro-ph/0312078.
- [18] S. Bottai, S. Giurgola, Astropart. Phys. 18 (2003) 539. Available from <arXiv:astro-ph/0205325>.
- [19] K. Giesel, J.-H. Jureit, E. Reya, Astropart. Phys. 20 (2003) 335. Available from <arXiv:astro-ph/0303252>.
- [20] J. Jones et al, hep-ph/0308042.
- [21] J. G. Learned, S. Pakvasa, Astropart. Phys. 3 (1995) 267. Available from <arXiv:hep-ph/9405296>.
- [22] H. Athar, G. Parente, E. Zas, Phys. Rev. D62 (2000) 093010. Available from <arXiv:hep-ph/0006123>.
- [23] S. I. Dutta, M. H. Reno, I. Sarcevic, Phys. Rev. D64 (2001) 113015. Available from <arXiv:hep-ph/0104275>.
- [24] J. F. Beacom et al., Phys. Rev. D68 (2003) 093005. Available from <arXiv:hep-ph/0307025>.
- [25] E. Bugaev, T. Montaruli, I. Sokalski, in: Proceedings of 28th International Cosmic Ray Conference, Tsukuba, 2003, p.1381. Available from <arXiv:astro-ph/0305284>.
- [26] E. Bugaev T. Montaruli, I. Sokalski, astro-ph/0311086.
- [27] R. J. Protheroe, in Accretion Phenomena and Related Outflows, ed. Wickramasinghe et al. (Astronomical Society of the Pacific, San Francisco, 1997).
- [28] K. Mannheim, R. J. Protheroe, J. P. Rachen, Phys. Rev. D63 (2001) 023003. Available from <arXiv:astro-ph/9812398>.
- [29] E. V. Bugaev, Yu. V. Shlepin, Phys. Rev. D67 (2003) 034027. Available from <arXiv:hep-ph/0203096>.
- [30] L. B. Bezrukov, E. V. Bugaev, Yad. Fiz. 32 (1980) 1636 [Sov. J. Nucl. Phys. 32 (1980) 847].
- [31] L. B. Bezrukov and E. V. Bugaev, Yad. Fiz. 33 (1981) 1195 [Sov. J. Nucl. Phys. 33 (1981) 635].
- [32] A. Dziewonski, *Encyclopedia of Solid Earth Geophysics*, ed. by D. E. James (Van Nostrand Reinhold, New York, 1989), p.331, we used the formula from this work cited in R. Gandhi et al., Astropart. Phys. 5 (1996) 81. Available from <arXiv:hep-ph/9512364>.
- [33] P. Lipari, M. Lusignoli, F. Sartogo, Phys. Rev. Lett. **74** (1995) 4384. Available from <arXiv:hep-ph/9411341>.

- [34] LEPTO package. Code and manual available from <<http://www3.tsl.uu.se/thep/lepto>>; G. Ingelman, A. Edin, J. Rathsmann, Comput. Phys. Comm. 101 (1997) 108. Available from <arXiv:hep-ph/9605286>.
- [35] B. Andersson et al., Phys. Rep. 97 (1983) 31.
- [36] JETSET and PYTHIA packages. Available from <<http://www.thep.lu.se/~torbjorn/Pythia.html>>; T. Sjöstrand, Comput. Phys. Comm. 82 (1994) 74.
- [37] H. L. Lai et al., Phys. Rev. D51 (1995) 4763. Available from <arXiv:hep-ph/9410404>.
- [38] H. Plöthow–Besch, Comput. Phys. Comm. 75 (1993) 396.
- [39] H. L. Lai et al., Phys. Rev. D55 (1997) 1280. Available from <arXiv:hep-ph/9606399>.
- [40] H. L. Lai et al., Eur. Phys. J. C12 (2000) 375. Available from <arXiv:hep-ph/9903282>.
- [41] J. Pumplin et al., JHEP 7 (2002) 12. Available from <arXiv:hep-ph/0201195>.
- [42] R. Gandhi et al., Phys. Rev. D58 (1998) 093009. Available from <arXiv:hep-ph/9807264>.
- [43] I. Sokalski, E. Bugaev, S. Klimushin, Phys. Rev. D64 (2001) 074015. Available from <arXiv:hep-ph/0010322>.
- [44] E. Gotsman, E. M. Levin, U. Maor, Eur. Phys. J. C5 (1998) 303. Available from <arXiv:hep-ph/9708275>.
- [45] A. D. Martin, M. G. Ryskin, A. M. Stasto, Eur. Phys. J. C7 (1999) 643. Available from <arXiv:hep-ph/9806212>.
- [46] A. N. Mueller, Nucl. Phys. B415 (1994) 373.
- [47] N. N. Nikolaev, B. G. Zakharov, Z. Phys. C49 (1991) 607.
- [48] J. R. Farshaw, G. Kerley, G. Shaw, Phys. Rev. D60 (1999) 074012. Available from <arXiv:hep-ph/9903341>.
- [49] S. I. Dutta et al., Phys. Rev. D63 (2001) 094020. Available from <arXiv:hep-ph/0012350>.
- [50] L. B. Bezrukov, E. V. Bugaev, in: Proceedings of 17th International Cosmic Ray Conference, Paris, 1981, Vol. 7, p. 102.
- [51] Yu. M. Andreev, L. B. Bezrukov, E. V. Bugaev, Yad. Fiz. 57 (1994) 2146 [Phys. At. Nucl. 57 (1994) 2066].
- [52] S. R. Kelner, Yu. D. Kotov, Sov. J. Nucl. Phys. 7 (1968) 237.

- [53] R. P. Kokoulin, A. A. Petrukhin, Acta Phys. Acad. Sci. Hung. 29, Suppl. 4, (1970) 277.
- [54] R. P. Kokoulin, A. A. Petrukhin, in: Proceedings of 12th International Cosmic Ray Conference, Hobart, 1971, Vol. 6, p. A2436.
- [55] S. R. Kelner, R. P. Kokoulin, A. A. Petrukhin, Yad. Fiz. 62 (1999) 2042 [Phys. Atom. Nucl. 62 (1999) 1894].
- [56] S. R. Kelner, Moscow Engineering Physics Inst. Preprint No. 016-97, 1997.
- [57] W. Lohmann, R. Kopp, R. Voss, CERN Report 85-03 (1985).
- [58] R. M. Sternheimer, Phys. Rev. 103 (1956) 511.
- [59] R. M. Sternheimer, R. F. Peierls, Phys. Rev. B3 (1971) 3681.
- [60] R. M. Sternheimer, M. J. Berger, S. M. Seltzer, Atom. Data Nucl. Data Tabl. 30 (1984) 261.
- [61] M. Derrick et al., Phys. Lett. B316 (1993) 412;
- [62] M. Derrick et al., Z. Phys. C65 (1995) 379;
- [63] M. Derrick et al., Z. Phys. C72 (1996) 399. Available from <arXiv:hep-ex/9607002>.
- [64] I. Abt et al., Nucl. Phys. B407 (1993) 515;
- [65] T. Ahmed et al., Nucl. Phys B439 (1995) 471. Available from <arXiv:hep-ex/9503001>;
- [66] H. Aid et al., Nucl. Phys B470 (1996) 3. Available from <arXiv:hep-ex/9603004>.
- [67] S. Jadach, J. H. Kuhn, Z. Was, Comput. Phys. Commun. 64 (1991) 275.
- [68] F. W. Stecker, M. H. Salamon, Space Sci. Rev. 75 (1996) 341. Available from <arXiv:astro-ph/9501064>.
- [69] J. Ahrens et al., Phys. Rev. Lett. 90 (2003) 251101. Available from <arXiv:astro-ph/0303218>.
- [70] J. Ahrens et al., astro-ph/0306209.
- [71] V. Aynutdinov et al., astro-ph/0305302.
- [72] V. A. Naumov, in: Proceedings of second Workshop on Methodical Aspects of Underwater/Underground Telescopes, Hamburg, 2001, p. 31. Available from <arXiv:hep-ph/0201310>.
- [73] G. Gelmini, P. Gondolo, G. Varieschi, Phys. Rev. D67 (2003) 017301. Available from <arXiv:hep-ph/0209111>.
- [74] T. S. Sinigovskaya, S. I. Sinigovsky, Phys. Rev. D63 (2001) 096004. Available from <arXiv:hep-ph/0007234>.
- [75] J. A. Aguilar et al., astro-ph/0310130.